Title

Mineralogical and transport controls on the evolution of porous media texture using direct numerical simulation

Journal

Water Resources Research, 53(5)

ISSN

0043-1397

Authors

Molins, Sergi
Trebotich, David
Miller, Gregory H
et al.

Publication Date

2017-05-01

DOI

10.1002/2016wr020323

Peer reviewed

Mineralogical and transport controls on the evolution of porous media texture using direct numerical simulation

Sergi Molins

David Trebotich

Gregory H. Miller

Carl I. Steefel
First published: 11 April 2017
https://doi.org/10.1002/2016WR020323
Cited by: 5
UC-eLinks

Abstract

The evolution of porous media due to mineral dissolution and precipitation can change the bulk properties of subsurface materials. The pore-scale structure of the media, including its physical and mineralogical heterogeneity, exerts controls on porous media evolution via transport limitations to reactive surfaces and mineral accessibility. Here we explore how these controls affect the evolution of the texture in porous media at the pore scale. For this purpose, a pore-scale flow and reactive transport model is developed that explicitly tracks mineral surfaces as they evolve using a direct numerical simulation approach. Simulations of dissolution in single-mineral domains provide insights into the transport controls at the pore scale, while the simulation of a fracture surface composed of bands of faster-dissolving calcite and slower-dissolving dolomite provides insights into the mineralogical controls on evolution. Transport-limited conditions at the grain-pack scale may result in unstable evolution, a situation in which dissolution is focused in a fast-flowing, fast-dissolving path. Due to increasing velocities, the evolution in these regions is like that observed under conditions closer to strict surface control at the pore scale. That is, grains evolve to have oblong shapes with their long dimensions aligning with the local flow directions. Another example of an evolving reactive transport regime that affects local rates is seen in the evolution of the fracture surface. As calcite dissolves, the diffusive length between the fracture flow path and the receding calcite surfaces increases. Thus, the calcite dissolution reaction becomes increasingly limited by diffusion.

1 Introduction

The use of subsurface environments in applications related to energy storage and security often involves the injection of fluids that are far from equilibrium with respect to the constituents of the native formation. Heterogeneous reactions driven by fluid-rock disequilibrium, such as mineral dissolution and precipitation, may change the properties of the porous medium, including porosity, permeability, and reactivity. In these applications, one is typically concerned

with the evolution of these properties at large scales. However, the changes take place at the scale of individual pores and grains, where small, localized effects may translate into significant impacts at larger scales via nonlinear emergent processes [*Ortoleva*, 1994]. Over the last decade, advances in characterization techniques and computational approaches have afforded an unprecedented look into how these changes play out at the pore scale [*Meakin and Tartakovsky*, 2009; *Steefel et al*., 2013; *Anovitz and Cole*, 2015].

Geologic sequestration of CO_2, an approach for mitigating greenhouse gas emissions, is one of these subsurface applications. In injecting CO_2 in the subsurface, one relies on the release of cations from native formation minerals via dissolution to drive precipitation of secondary carbonate minerals, effectively trapping carbon in the subsurface [*Steefel et al*., 2013]. Pore-scale investigations into the interactions of CO_2-rich fluids with porous media have focused on the effects of pore structure and heterogeneity on reaction rates [*Li et al*., 2007; *Molins et al*., 2012] and on the development of the reactive infiltration instability as a result of the fast carbonate dissolution rates driven by CO_2 [*Golfier et al*., 2002; *Szymczak and Ladd*, 2009; *Smith et al*., 2013; *Ott and Oedai*, 2015]. The reactive infiltration instability—also extensively investigated in works on acidification of hydrocarbon reservoirs for enhanced oil recovery [*Hoefner and Fogler*, 1988; *Cohen et al*., 2008]—is a form of geochemical self-organization or pattern formation that is characteristic of advection-dominant reactive flow systems [*Ortoleva*, 1994]. This occurs where mineral dissolution under transport-controlled conditions leads to the more rapid growth of high-flow velocity pathways at the expense of slower flow pathways.

Transport control of rates within individual pore spaces and around mineral surfaces has also been the subject of recent studies [*Li et al*., 2008; *Noiriel et al*., 2012; *Molins et al*., 2014; *Rimstidt*, 2015; *De Baere et al*., 2016]. Diffusive transport to mineral surfaces, particularly in physically and mineralogically heterogeneous porous media, can lead to poorly mixed conditions within the pore space. Dissolution of calcite is relatively rapid compared to transport rates under the typical flow conditions of subsurface environments. At the spatial scale of individual pores (micrometer to hundreds of micrometer), this implies that diffusive transport to mineral surfaces may be limiting the effective dissolution rate. As a result, mineral grain surfaces in close proximity may be subject to different reactive regimes due to pore-scale variations of the flow velocity; areas of the grain surface thus contribute little to the overall dissolution rate in the case where slow flow allows for closer-to-equilibrium conditions locally [*Molins et al*., 2014; *De Baere et al*., 2016]. As a result, these nonuniform rates at mineral

surfaces may result in nonuniform evolution of mineral grains [*Rycroft and Bazant*, 2016], thus affecting the texture of porous media.

In mineralogically heterogeneous media, the evolution of the texture also depends on the mineral assemblage and its spatial distribution as shown by recent experimental and modeling studies in fractured carbonate rocks subject to high CO_2 conditions [*Ellis et al*., 2011; *Deng et al*., 2013, 2016; *Wen et al.*, 2016]. The evolution of the fracture surface can be strongly influenced by the spatial assemblage of the faster-dissolving calcite and the slower-dissolving dolomite, resulting in the development of nonuniform dissolution patterns and altered porous layers [*Ellis et al*., 2011]. Hydrologic accessibility to reactive phases can add to this effect. For example, when micropores are not connected to the macropores within which most of the flow occurs, the minerals in these micropores contribute little or nothing to the overall reactivity [*Peters*, 2009; *Landrot et al*., 2012].

Many of these issues can be addressed with pore-scale modeling. Approaches to pore-scale modeling of reactive geochemical systems include pore network models [*Li et al*., 2007], the lattice Boltzmann method [*Yoon et al*., 2015], and particle methods [*Tartakovsky et al*., 2007]. Direct numerical simulation involves the use of conventional discretization methods that include Eulerian, mesh-based finite-difference, finite-element, or finite-volume methods. A feature of direct numerical simulation is the need to explicitly incorporate a description of the solid-fluid interfaces. While gridding schemes that conform to the domain boundary, e.g., unstructured grid methods, can capture complex interface geometries by appropriate meshing strategies, remeshing is required when solid-fluid interfaces evolve due to dissolution-precipitation reactions. In contrast, structured-mesh models require a method to represent the interfaces such as the immersed boundary method [*Benioug et al*., 2015] or the embedded boundary method [*Miller and Trebotich*, 2012; *Molins*, 2015]. The embedded boundary method, which uses cut cells that result from intersecting the irregular fluid-solid interfaces with structured Cartesian grids, makes it possible to take advantage of structured methods while capturing complex surficial geometries [*Trebotich et al*., 2014; *Trebotich and Graves*, 2015]. This method has previously been successfully used to simulate reactive transport processes at the pore scale in complex nonevolving pore space geometries [*Molins et al*., 2014; *De Baere et al*., 2016].

In this paper, a new pore-scale model for the evolution of solid-fluid interfaces is developed to investigate the changing texture of porous media subject to dissolution-precipitation. The model builds on an existing embedded-boundary structured-mesh code [*Molins et al*., 2012; *Trebotich and Graves*, 2015] and incorporates a method for the solution of the flow and reactive transport equations on time-dependent domains [*Miller and Trebotich*, 2012]. The emphasis is placed on

investigating the flow and transport controls on the textural evolution of porous media at the scale of individual pores. We start with simple one and two-grain domains before moving on to an assembly of a larger number of grains. In the latter, pore-scale textural changes coexist and interact with larger-scale processes such as the rapid growth of high-flow velocity pathways in the porous medium domain. The effect of mineralogical heterogeneity is then explored with a fracture model that simulates observations by Ellis and coworkers [*Ellis et al.*, 2011].

2 Model Description

The problem considered in this work entails the solution of the coupled processes of fluid flow, multicomponent reactive transport, and geometry evolution. The fluid-solid interface (Γ) is assumed to be sharp and impermeable to flow. Flow and reactive transport are thus solved only in the pore space and boundary conditions are applied at the solid-fluid boundaries. Flow is described by the Navier-Stokes equations for incompressible flow

$$\frac{\partial \boldsymbol{u}}{\partial t} + (\boldsymbol{u} \cdot \nabla)\boldsymbol{u} + \frac{1}{\rho}\nabla p = \nu \Delta \boldsymbol{u}, \quad (1)$$

$$\nabla \cdot \boldsymbol{u} = 0, \quad (2)$$

where **u** is the fluid velocity, ∇p is the pressure gradient, and ν is the kinematic viscosity. Transport is simulated with the multicomponent advection-diffusion equation

$$\frac{\partial \psi_i}{\partial t} + \nabla \cdot \boldsymbol{u}\psi_i = \nabla \cdot D_i \nabla \psi_i, \quad (3)$$

where ψ_i is the total molar concentration of component *i*, and D_i is the diffusion coefficient of component *i* in the fluid. Aqueous complexation reactions are assumed to be at equilibrium and modeled with the mass action law, which allows one to define the total component concentration (ψ_i) as the sum of the molal concentration of a primary species (c_i) and a set of the secondary species (m_i)

$$\psi_i = \rho \left(c_i + \sum_{j=1}^{N_x} \xi_{ji} m_j \right), \quad (4)$$

where ρ is the fluid density, ξ_{ji} is the stoichiometric coefficient of species *i* in reaction *j*, and N_x is the number of aqueous equilibrium reactions. Mineral dissolution is described as a kinetic process with its rate described explicitly as a function of the species concentrations. At the pore scale, this rate is a surface rate, is calculated at the mineral-fluid interface, and thus can be expressed as a boundary condition

$$-\rho D_i \nabla c_i = \sum_m \chi_m \xi_{mi} r_m(c), \quad (5)$$

where r_m is the surface dissolution rate [mol/m^2/s], and ξ_{mi} is the stoichiometric coefficient of species *i* in the mineral reaction *m*. The reactive surface area is assumed to be equal to the physical fluid-solid interfacial area [*Molins et al.*, 2012] and appears in the discretized form of the equations. In equation 5, χ_m is the fraction of the surface composed of mineral *m* such that

$\sum_m \chi_m = 1$. In the simulations in this manuscript, mineral composition is not resolved below the spatial resolution of the domain. That is, within each grid cell $\chi_m = 0$ or 1.

The velocity of the moving solid-fluid interface normal to the interface (v_n^Γ) can be described by [e.g., *Li et al*., 2010]

$$v_n^\Gamma = \sum_m \chi_m V_m r_m, \quad (6)$$

where V_m is the molar volume of the *m*th mineral [m³/mol]. As the geometry evolves, parameters associated with this geometry such as the value of the reactive surface area also change.

Equations 1-6 describe a set of coupled processes that interact with one another.

Equation 6modifies the geometry of the domain, thus affecting the boundary conditions both for reactive transport (equation 5), as well as for flow

$$\boldsymbol{v} = v_n^\Gamma \boldsymbol{n} \text{ on } \Gamma. \quad (7)$$

In the calculation of the mineral reaction rates, the Transition State Theory (TST) rate law [*Lasaga*, 1981] is used. For calcite dissolution, the reaction focus of this paper, the surface rate can be written as [*Plummer et al*., 1978; *Chou et al*., 1989]

$$r_m = (k_1 a_{H^+} + k_2 a_{H_2CO_3^*} + k_3)\left(1 - \frac{a_{Ca^{2+}} a_{CO_3^{2-}}}{K_{s,cal}}\right), \quad (8)$$

where $K_{s,cal}$ is the equilibrium constant of the reaction; a_{H^+}, $a_{HCO_3^-}$, $a_{CO_3^{2-}}$, and $a_{Ca^{2+}}$ are the species activities; and k_1, k_2, and k_3 are rate constants. Considerable uncertainty is associated with reaction rate parameters, often over orders of magnitude, especially as reflected by the so-called discrepancy between laboratory and field rates [e.g., *Maher et al*., 2006]. As a result, Darcy-scale modeling studies often resort to using the reactive surface area as calibration parameter to match observations. In the pore-scale approach, however, the reactive surface area is derived from the geometry of the mineral-fluid interface and often, as done here, assumed to be equal to the physical area of this interface [*Molins*, 2015]. Recent pore-scale simulations using this assumption and literature-derived rate parameters have shown good agreement to data from single calcite grain experiments [*De Baere et al*., 2016] and grain pack experiments [*Molins et al*., 2014]. Using rate data from *Pokrovsky et al*. [2005], *Molins et al*. [2014] reported a discrepancy by a factor of 1.8 between simulated and measured concentrations, also attributed in part to transport limitations to reactive surfaces. *De Baere et al*. [2016] obtained a remarkably good agreement effluent concentrations using the parameter values of *Chou et al*. [1989]. Because the use of equation 8 at the pore scale on the surface of the mineral carries the assumption that k_1, k_2, and k_3 are obtained experimentally under strict surface controlled conditions [*Molins et al*., 2014], the fluidized bed reactor with ground mineral samples employed by *Chou et al*. [1989] or the fast-rotating disk reactor of *Pokrovsky et al*. [2005] provide rate data that are expected to reduce uncertainty when applied as surface rates in pore-scale models.

Dissolution of calcite contributes to the mass of dissolved components via equation 5according to the following stoichiometric relationship:

$$CaCO_3(s) \rightarrow Ca^{2+} + CO_3^{2-} \quad (9)$$

While flow, transport, reactions, and boundary displacement are coupled processes, the time scales associated with each one of them can be dramatically different, with

$$t_V = L^2/\nu; \quad t_A = L/U; \quad t_D = L^2/D; \quad t_R = LC_0/R; \quad t_B = \frac{L}{RV_m}, \quad (10)$$

being the time scales of viscous, advective, diffusive, reaction, and boundary displacement processes, respectively. In equation 10, L, U, D, and R are the characteristic length, fluid velocity, diffusion coefficient, and surface reaction rate, and C_0 is a reference concentration, e.g., the concentration of a species at equilibrium with the mineral.

For calcite dissolution, under the range of spatial dimensions and inlet fluid velocities considered in this study, the rate of the (mineral-fluid) boundary displacement is much slower than that of the processes of flow and reactive transport. As such, we solve for each of these processes separately over a time step Δt_b, with the assumption that geometry changes have a negligible effect on the flow and transport solutions over this time step. This allows us to update the geometry based on a reaction rate that does not change over the duration of a given time step. The size of this time step is chosen as a fraction ($0 < f < 1$) of the CFL-constrained time step for boundary displacement. The CFL (or Courant-Friedrich-Levy) condition limits the time step size based on the grid size (Δx) such that

$$\Delta t_b \leq f \frac{\Delta x}{\max_i |v_n^\Gamma|} \quad (11)$$

In other words, the maximum geometry displacement allowed is a fraction of the grid size. For the simulations presented in this manuscript: $f = 0.25$. The solutions of flow and reactive transport are obtained via subtime stepping within this Δt_b with time steps constrained by the viscous time scale ($\Delta t_V = \Delta x^2/\nu$) for flow and by the CFL criterion ($\Delta t_A = \Delta x / \max_i |u_i|$) for transport. Relaxation times for flow and transport are short compared to Δt_b and steady state for flow and transport is reached for a time increment (Δt^*) that is much smaller than Δt_b, such that $\Delta t_V < \Delta t_A < \Delta t^* < \Delta t_B$. The solution is carried out sequentially, that is, flow (equations 1 and 2) is solved first using the velocity of the interface in the previous time step as boundary condition (equation 7). Then, reactive transport (equations 3-5 and 8) is solved using the fluid velocities obtained from the solution of the flow problem. Finally, the solid-fluid interface is moved according to the local dissolution rate via equation 6.

3 Transport Controls on Surface Evolution

3.1 At the Grain Scale

A set of simulations is performed to explore the effect of flow and the relative importance of advective and diffusive transport on the evolution of mineral surfaces in simple domains. In these simulations, one or two calcite crystals are placed in cross-flow conditions in a 2-D rectangular channel. For convenience, the grains have a cylindrical shape with their radius equal to 0.01 cm, or 1/5 of the width of the flow channel (Figure 1). A solution, at pH 5, out of equilibrium with respect to calcite (Table 1) [*Li et al*., 2008; *Molins et al*., 2012], flows into the domain and drives dissolution of the grain. Because of dissolution, the concentrations of product species such as calcium increase around and downstream of the mineral grains. The parameter values obtained by *Chou et al*. [1989] at 25°C—$k_1 = 0.89$, $k_2 = 5.01 \times 10^{-4}$, and $k_3 = 6.6 \times 10^{-7}$ mol m^{-2} s^{-1}—are used in equation 8 owing to the good agreement found in the experimental/modeling study of *De Baere et al*. [2016]. The top and bottom walls of the channel are assumed to be no-slip boundaries (the fluid velocity is zero at the boundary) representing potential flow constrictions located in the proximity of the grain. The domain is discretized using 256 × 128 grid cells (resolution of 3.91 μm). A uniform velocity boundary condition is applied over the inlet face that determines the volumetric flux (equal in value to the inlet velocity as the inlet face is fully porous) and the flow rate through the domain. The value of this inlet velocity is varied (0.0012, 0.012, 0.12, and 1.2 cm/s) to explore a range of conditions that change the balance between the different processes involved. For all velocities in the range explored, advection is dominant over diffusion with a Péclet number ($Pe = \frac{t_D}{t_A}$) greater than 1, increasingly so with increasing inlet velocity (Table 2). In parallel, the advective Damköhler number ($Da_I = \frac{t_A}{t_R}$) decreases from values greater than 1 for 0.0012 cm/s to less than 1 for 0.012, 0.12, and 1.2 cm/s. This indicates that for the slower flow rates the reaction rate is fast relative to the rate of delivery of reactants or removal of products. This means that the minerals and solution can potentially reach equilibrium over the length scale of interest (L) in this case the diameter of the grain (Φ). Near the grain boundary, however, the velocity decreases and diffusion dominates. The diffusive Damköhler number ($Da_{II} = \frac{t_D}{t_R}$) is equal to 7.6 in all cases, indicating that diffusion determines the steady state gradients near the grain boundary.

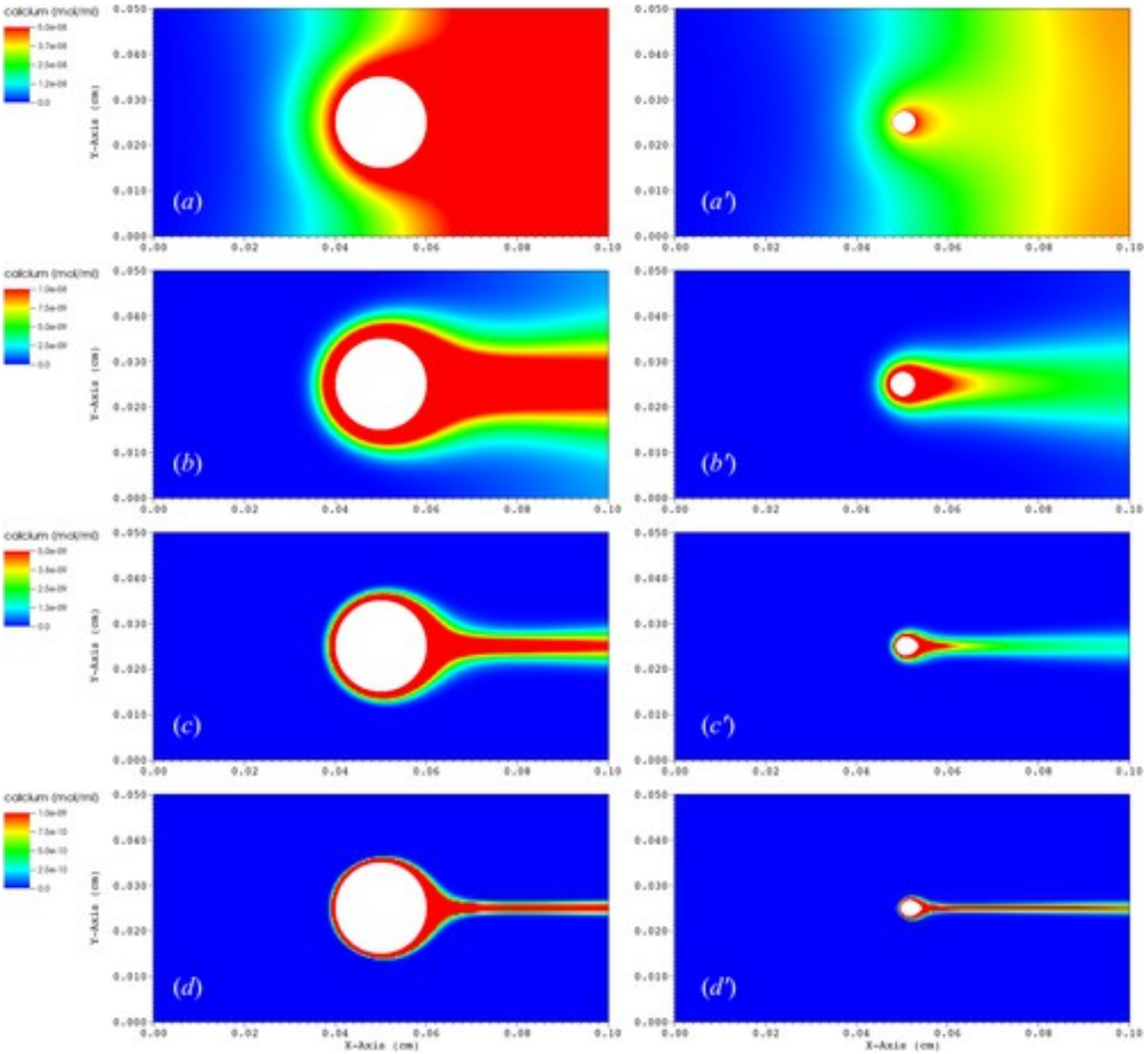

Figure 1

[Open in figure viewerPowerPoint]

Calcium concentrations around a dissolving grain of calcite at steady state conditions for reactive transport for a range of prescribed inlet fluid velocities: (a, a′) 0.0012 cm/s, (b, b′) 0.012 cm/s, (c, c′) 0.12 cm/s, and (d, d′) 1.2 cm/s. Figures 1a–1d show conditions that correspond to the initial grain size, and Figures 1a′–1d′ show later stages of the evolution, namely, t = 909, 820, 696, and 438 h, respectively.

Caption

Table 1. Solution Parameters Used for Initial and Inlet Boundary Conditions in the Simulations of Dissolution of One and Two-Grain Domains and Array Pack Domains

Parameter	Value
pH	5.0
Cl	1.0011×10^{-2} mol/kgw
pCO_2	3.15×10^{-4} bar
Ca	0.0 mol/kgw
Na	1.0×10^{-2} mol/kgw

Table 2. Summary of Dimensionless Numbers for the Simulations Based on Initial Geometry Dimensions

Simulation	Péclet (Pe)	Advective Damköhler (Da_I)	Diffusive Damköhler (Da_{II})
One and Two Crystals			
v = 0.0012 cm/s	2.4	3.173	7.6
v = 0.012 cm/s	24.0	0.317	7.6
v = 0.12 cm/s	240.0	0.032	7.6
v = 1.2 cm/s	2400.0	0.003	7.6

Simulation	Péclet (Pe)	Advective Damköhler (Da_I)	Diffusive Damköhler (Da_{II})
Grain Arrays (All)			
v = 0.01 cm/s	500	0.381	190
v = 0.1 cm/s	5000	0.038	190
Fracture			
v = 110 cm/h	53.1	0.008 (calcite)	0.43 (calcite)
v = 110 cm/h	53.1	1.65×10^{-4} (dolomite)	0.009 (dolomite)

Because of the interplay between advection, diffusion, and reaction, the relative magnitude of the rate of dissolution on the different grain surfaces is different under the range of conditions considered. At slow inlet velocities, the rate is approximately the same on all grain surfaces (Figures 2a and 2b). The original cylindrical grain retains its shape as the mineral surfaces dissolve at the same rate everywhere along the mineral surface. At faster velocities, the rate—in addition to being more rapid on average than in the slow-flow cases—is greater on the upgradient surfaces than on the downgradient surfaces where the increase in pH and/or the approach to chemical equilibrium slows the rate (Figures 2c and 2d). Thus, the grain surface recedes more slowly on the downgradient side of the grain. In the process, the center of mass of the grain moves downgradient with this migration being greater at faster flow velocities (Figure 2). In the slow flow rate scenarios (greater Da_I values), the reaction is fast compared to the rate of input of reactants and removal of products. This implies that dissolution at all surfaces of the grain is largely controlled by diffusion in the boundary layer, with pH at the surface nearing the equilibrium value (9.75) within one pH unit (Figure 3). Conditions at the surface are then dominated by the zero-order term of the kinetic reaction (i.e., $k_3 \gg k_1 \ a_{H^+}$), and the reaction rate depends on the surface concentrations via the near-equilibrium term. At faster flow

rates, in contrast, a difference is observed between upgradient and downgradient surfaces. While downgradient surfaces experience conditions like those in the slow flow simulations, upgradient surfaces remain far from equilibrium (Figure 3). The dissolution rate at these upgradient surfaces is controlled by surface processes to a greater extent than it is on the downgradient surfaces, with the $k_1 \ a_{H^+}$ term dominating the rate.

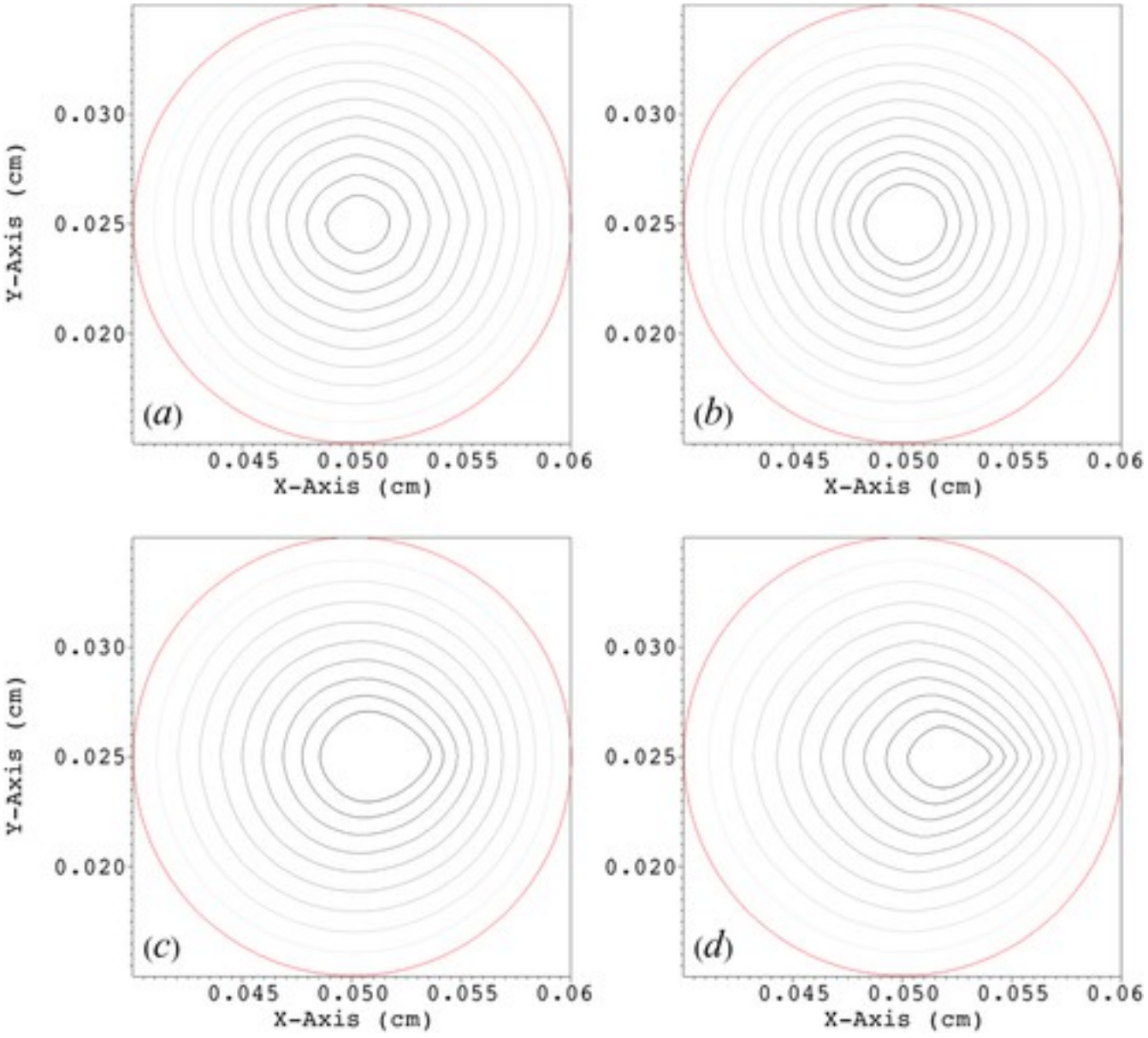

Figure 2

Open in figure viewerPowerPoint

Evolution of a single calcite grain at a range of inlet fluid velocities (a) 0.0012 cm/s, (b) 0.012 cm/s, (c) 0.12 cm/s, and (d) 1.2 cm/s. In red is the original grain boundary, and later stages are shown as a gray scale with increasing shade with time.

Caption

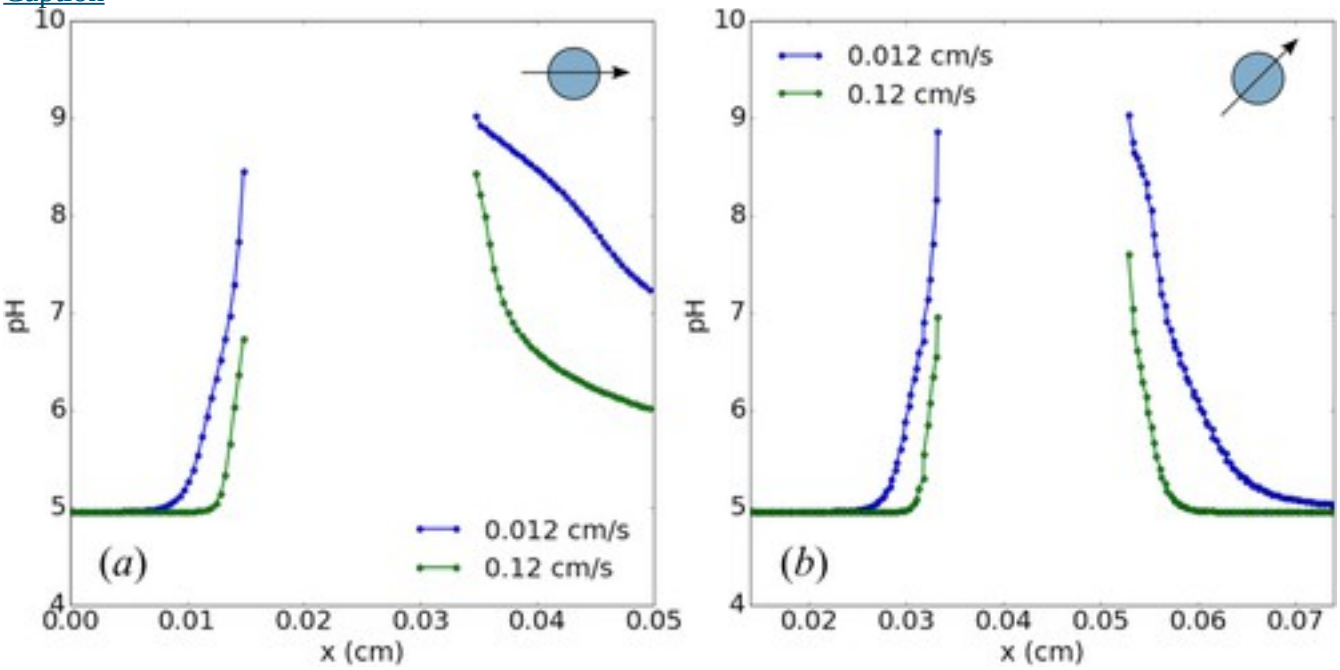

Figure 3

Open in figure viewerPowerPoint

pH values plotted along (a) a horizontal line and (b) a line at 45° with the horizontal, for two flow conditions, showing the thickness of the local diffusive boundary at steady state conditions for reactive transport with the initial grain size (i.e., Figure 1, left). The gap in values indicates the presence of the mineral grain.

Caption

In this simple domain, the flow field is symmetrical around the grain and the part of the surface of the grain facing the inflowing solution directly dissolves the fastest. In general, the spatial arrangement of the grains within a porous medium affects the flow field, which results in different rates on different surfaces [e.g., *Molins et al.*, 2014]. We consider now a two-grain domain of the same size as the single-grain domain subject to the same inlet conditions for two prescribed inlet velocities: 0.012 and 0.12 cm/s (Figure 4), representative of relatively slow and relatively fast flow conditions, respectively. For the inlet velocity of 0.012 cm/s, the evolution of the grains is similar to that in the single-grain case, with the cylindrical grain keeping its shape as its surfaces evolved (Figure 4). This is an indication of similar diffusion control on rates on all surfaces. In contrast, for the inlet velocity of 0.12 cm/s, the mineral dissolves relatively more rapidly at the surfaces exposed to the fast flow path (in the pore throat between the grains). At these surfaces, diffusive boundary layers are thinner and conditions are far from equilibrium, indicating a mixed control on the rates. At the surfaces exposed to slow-flowing paths and on the downgradient side of the grains, the rate is relatively slower, with rates mostly controlled by

diffusion and conditions nearing equilibrium with calcite (Figure 4). The overall result is that grains evolve to oblong shapes, with their long dimensions aligning with the local flow directions (Figure 4).

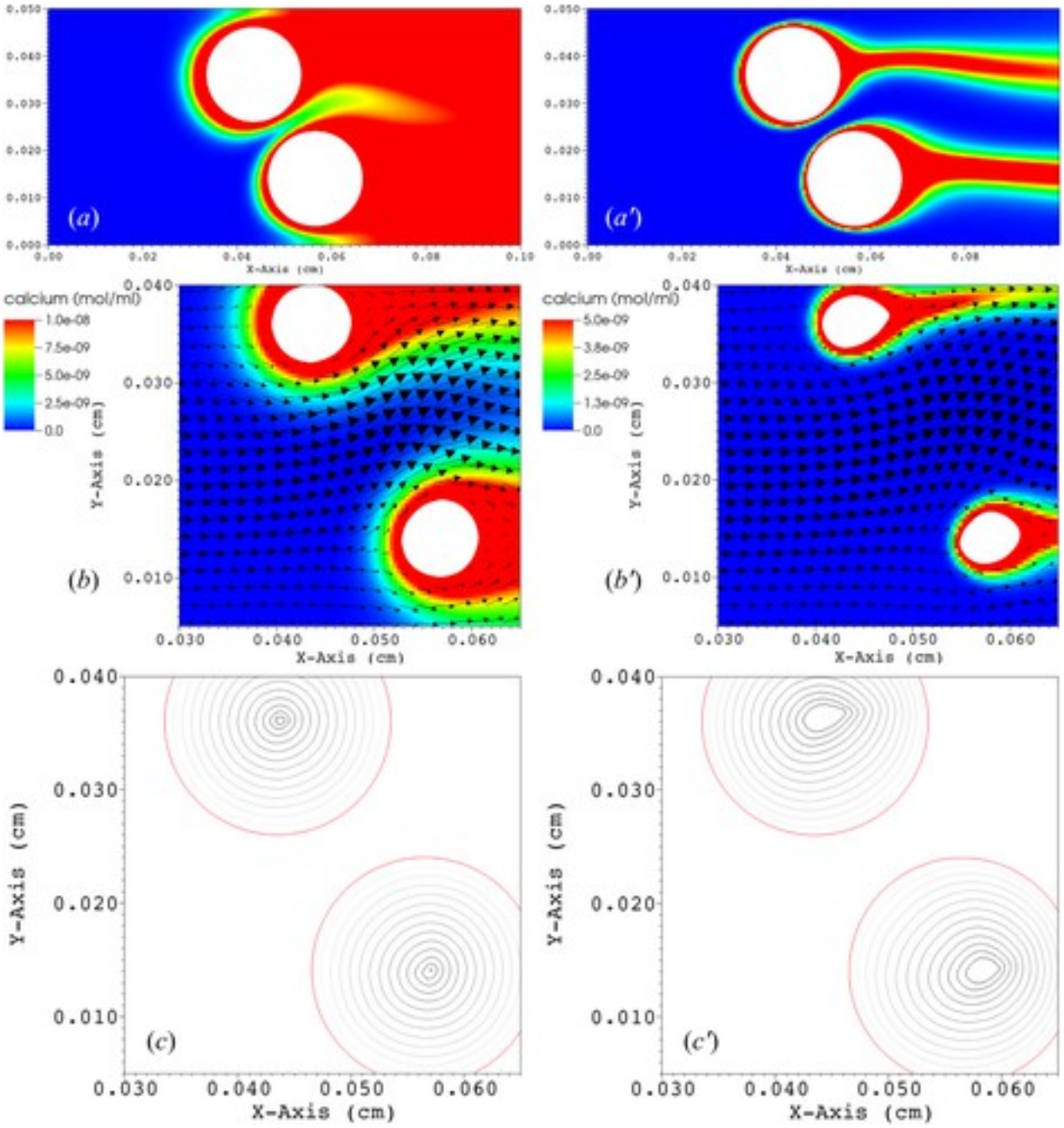

Figure 4

Open in figure viewerPowerPoint

Results for the two-grain simulations at two prescribed inlet fluid velocities: (a, b, c) v = 0.012 cm/s and (a′, b′, c′) v = 0.12 cm/s. (a, a′) Calcium concentrations at steady state conditions for reactive transport with the initial grain size, in the entire simulation domain. (b, b′) Calcium

concentrations at steady state conditions for reactive transport at later stages of grain evolution (673 h in Figure 4b and 606 h in Figure 4b′), with vectors showing local fluid velocities and relative magnitudes, in the pore throat region of the domain. (c, c′) Evolution of the grain surfaces with time: in red is the initial grain boundary, and later stages are shown as a gray scale with increasing shade with time.

Caption

3.2 At the Grain-Pack Scale

In this section, we revisit the set of simulations presented in *Molins et al*. [2012] in which three two-dimensional, 1 cm long 0.5 cm wide domains were packed with 378 cylindrical grains. In one of the domains, the grains are uniformly distributed as a staggered array (Figure 5a); in a second, calcite grains are randomly packed so as to produce a more heterogeneous medium (Figure 5b); and in a third, calcite grains are packed randomly in two distinct zones, with tighter and looser packing in the upper and lower half, respectively (Figure 5c). The grains represent calcite that dissolves as the undersaturated solution flows left to right through the domain. The three domains have equivalent average geochemical parameters: the cylinder radii are 0.01 cm—the same as in the one and two-grain simulations above—resulting in a porosity of 0.76, and calcite-specific surface area for the domain of 4750 m^2/m^3. While a porosity value of 0.76 is not to be expected in geological formations it is used in these two-dimensional domains to ensure a minimum separation between grains in the tight packing of the top half of the two-zone domain (Figure 5c). Two scenarios are considered: one equivalent to the simulations in *Molins et al*. [2012] with an inlet velocity of 0.1 cm/s (Figure 5) and another with an inlet velocity of 0.01 cm/s (Figure 6). These simulations result in the distribution of velocities shown in Figure 7, with the median of pore space velocities in each case (0.12 and 0.012 cm/s) used as inlet velocities in the corresponding simulations presented in the previous section. The domain is discretized using 2048 × 1024 grid cells in all cases for a resolution of 4.88 μm.

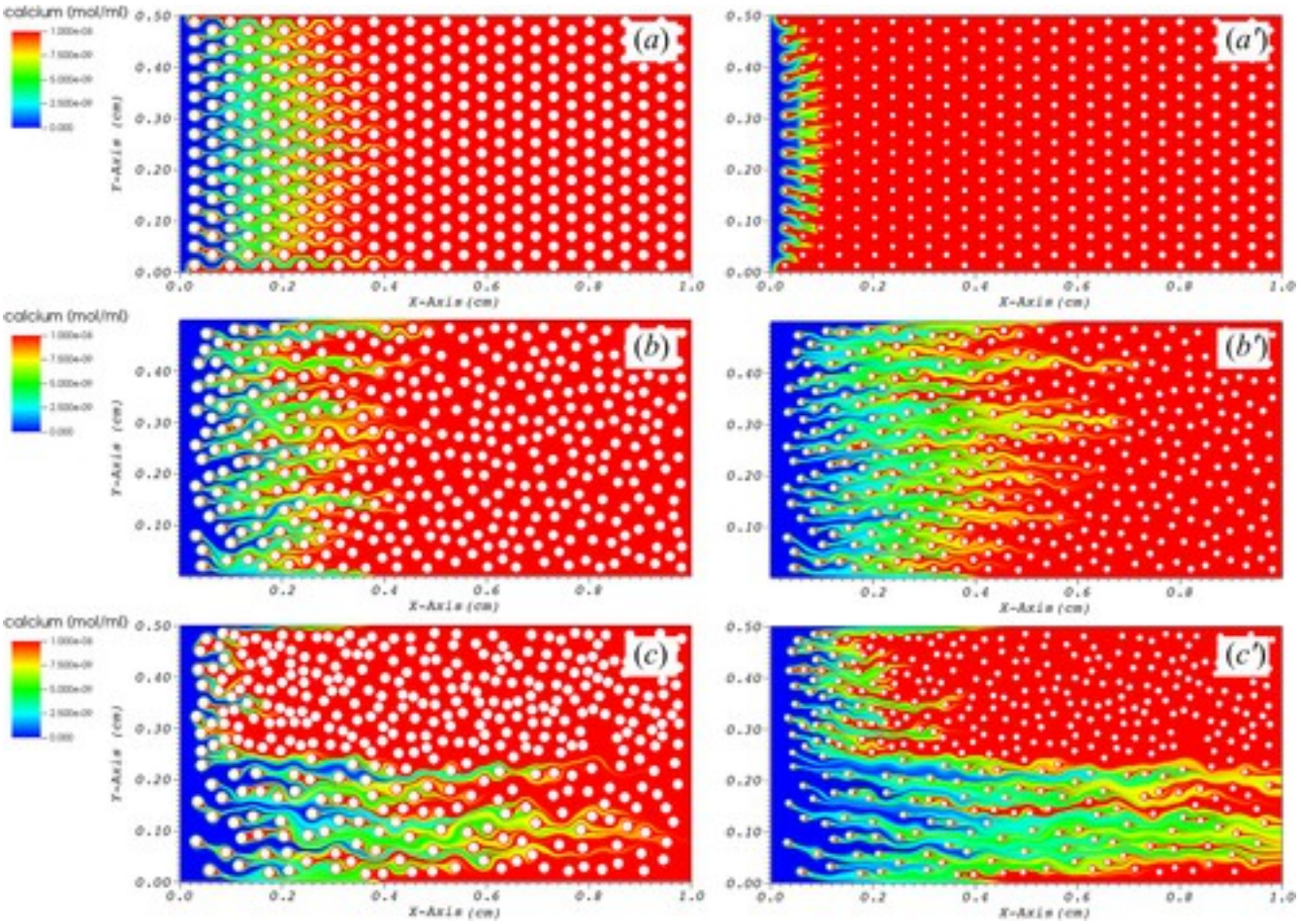

Figure 5

Open in figure viewerPowerPoint

Calcium concentrations at steady state conditions for reactive transport for a prescribed inlet fluid velocity of 0.12 cm/s in three grain packings: (a, a′) uniform, (b, b′) heterogeneous and (c, c ′) two-zone packing. Figures 5a–5c show conditions that correspond to the initial geometry, and Figures 5a′–5c′ show a later stage of the evolution, namely, t = 576 h, 588 h, and 468 h, respectively.

Caption

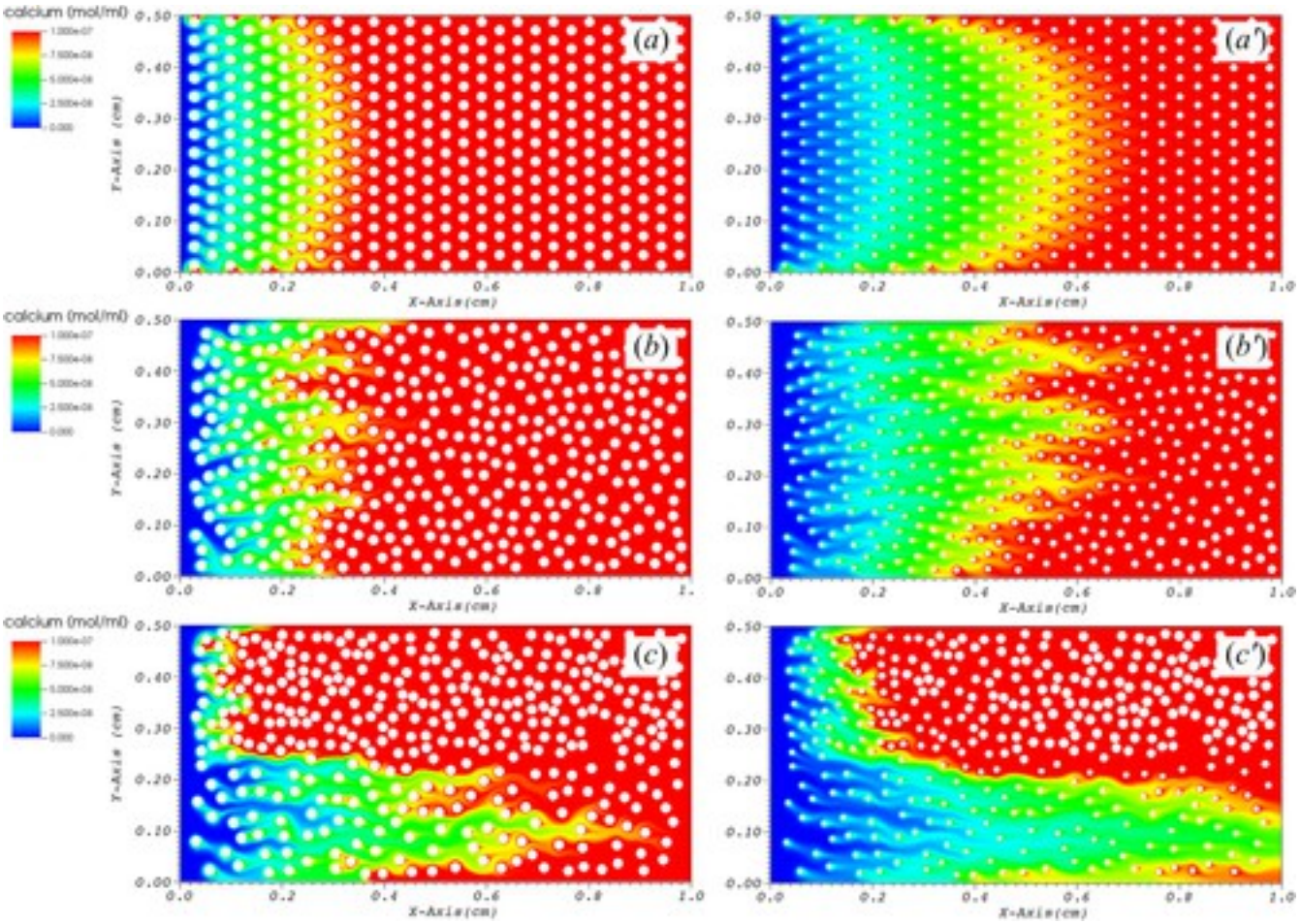

Figure 6

Open in figure viewerPowerPoint

Calcium concentrations at steady state conditions for reactive transport for a prescribed inlet fluid velocity of 0.012 cm/s in three grain packings: (a, a′) uniform, (b, b′) heterogeneous, and (c, c′) two-zone packing. Figures 6a–6c show conditions that correspond to the initial geometry, and Figures 6a′–6c′ show a later stage of the evolution, namely, t = 639 h, 593 h, and 572 h, respectively.

Caption

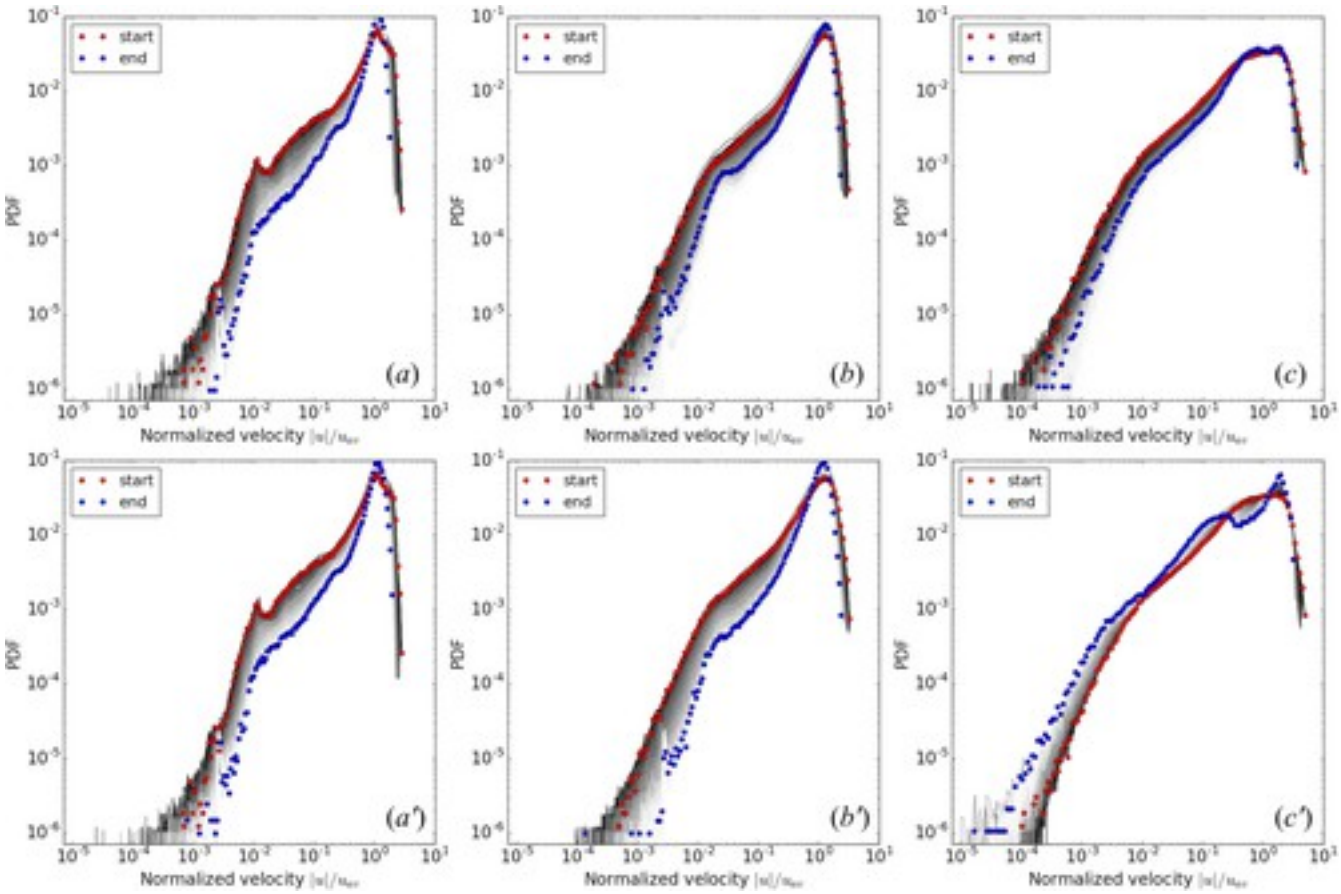

Figure 7

Open in figure viewerPowerPoint

Initial (red) and final (blue) fluid velocity distributions in three grain packings: (a, a′) uniform, (b, b′) heterogeneous, and (c, c′) two-zone packing. Intermediate distributions are shown as gray-scale values with intensity decreasing with time. Figures 7a–7c are for a prescribed inlet fluid velocity of v = 0.1 cm/s, while Figures 7a′–7c′ are for v = 0.01 cm/s.

Caption

At an inlet velocity of 0.1 cm/s, the textural evolution of the grain packing is similar in all three domains (Figure 5). Under these conditions, an advective Damköhler number (Da_l, L = width) of 0.038 makes it apparent that the time scales associated with advective transport are shorter than with reaction. Therefore, the rate of change in grain size is very similar along the domain, being only slightly faster near the inlet and decrease with increasing distance from the inlet. As reactants are consumed and the concentrations of the product species increase downgradient, the rate decreases with distance from the inlet. In all three cases, the distribution of velocities changes in a similar way, with velocities becoming more uniform (increased median velocity peak and decreased slow-velocities tail, Figure 7).

Near the inlet, conditions are similar to those in the one and two-grain simulations presented earlier at a prescribed inlet velocity of 0.12 cm/s. Thus, the evolution of shape of the grains is consistent with that observed in the results presented above. That is, the overall evolved texture shows grains with elongated shapes aligned with the local flow direction (Figure 8a). As reactants are consumed and concentrations of product species increase downgradient, the driving force for reaction decreases. As noted by *Molins et al*. [2012], under these conditions the rate is dominated by a reaction pathway associated with a zero-order dependence on k_3. The rate is uniform on the surface of each individual grain and the shape does not change as the grain dissolves (Figure 8b).

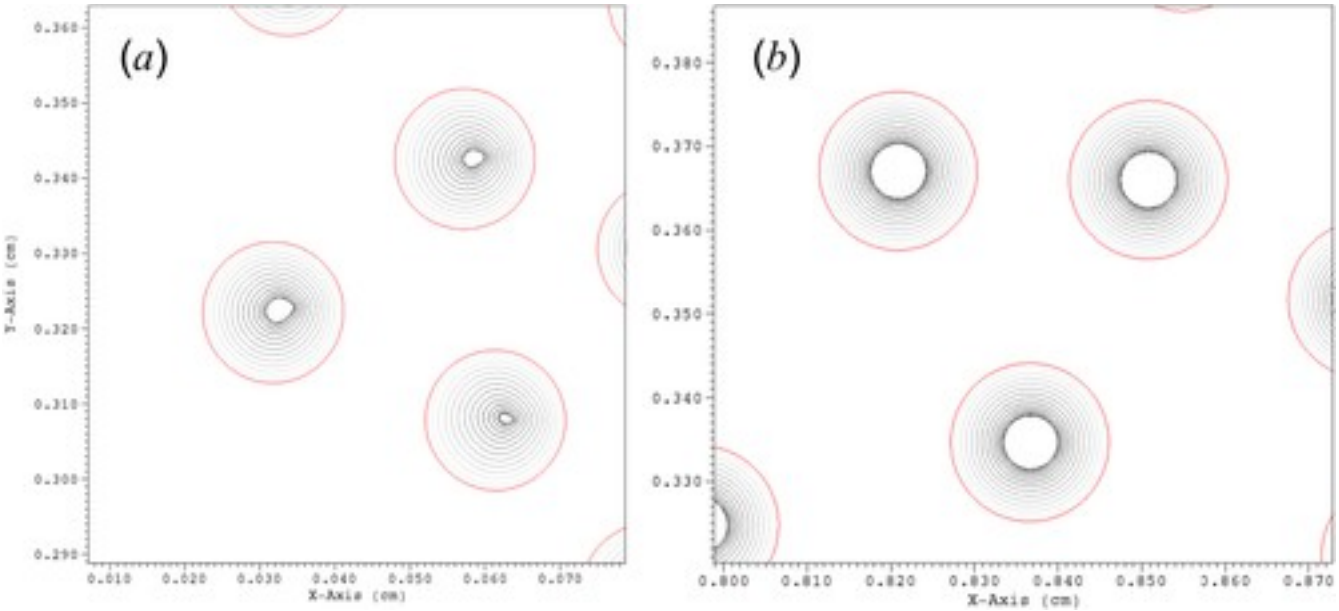

Figure 8

Open in figure viewerPowerPoint

Evolution of the grain boundary geometry in two selected sections of the heterogeneous grain packing located (a) near the inlet and (b) near the outlet for a prescribed inlet fluid velocity of v = 0.1 cm/s. In red is the initial grain boundary; later stages are shown as a gray scale with shade increasing with time.

Caption

At an inlet velocity of 0.01 cm/s, the time scales associated with reaction in the domain are more similar to those expected where advective transport dominates (Da_I = 0.38). The evolution of the three domains is different. While the staggered array and the heterogeneous packings evolve similarly as in the case of slow velocities, in the two-zone packing a fast flow path develops in the high-permeability zone. Thus, the velocity distribution becomes more bimodal over time, with a decreased median velocity peak and a secondary peak appearing for slow velocities

(Figure 7c). Dissolution in this domain takes place preferentially in the fast flow path already present in the initial pore structure, thus driving in turn faster flow there and hence more rapid dissolution in a self-organizing phenomenon as a result of the reactive infiltration instability [*Ortoleva*, 1994].

Because of the development of this fast flow path, the evolution of the shape of each individual grain in the domain cannot be predicted based solely on results from the one and two-grain simulations at slow flow rates. In the staggered array and randomly packed domains, the grains both near the inlet and outlet maintain their cylindrical shape as the dissolution rate on each individual grain is uniform (not shown). This agrees with the evolution of the individual grains in the simulations presented in the earlier section run at 0.012 cm/s. However, in the two-zone heterogeneously packed domain, and because of the increase in velocities in the flow path, some grains are subject to conditions closer to those that lead to the development of elongated grain shapes (Figure 9b). These grains are in regions of fast flow paths and experience concentrations like those at the inlet. Grains in the slow-flowing regions dissolve at significantly slower rates, as rates are limited by slow transport of the influent solution into these regions, and the grains keep their shape as they dissolve (Figure 6). This is in contrast with what occurs when the inlet velocity is 0.1 cm/s where conditions at the grain scale are not transport-limited, the fast flow path does not develop and grain shape evolution depends on the distance from the inlet (e.g., uniform evolution in the region shown in Figure 9a).

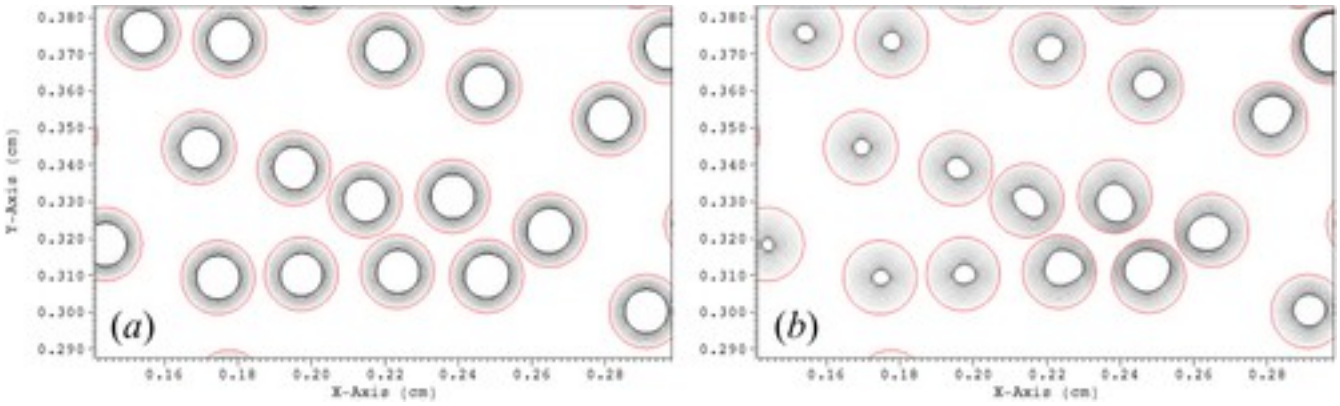

Figure 9
Open in figure viewerPowerPoint
Evolution of the grain boundary in a selected region of the two-zone grain packing domain for a simulation with a prescribed inlet fluid velocity of (a) 0.1 cm/s and (b) 0.01 cm/s. In red is the initial grain boundary; later stages are shown as a gray scale with shade increasing with time.

Caption

4 Mineralogical Controls on Surface Evolution

While the effect of transport limitations on the textural evolution is apparent in the geometrically and chemically simple simulations presented in the previous sections, the physical and mineralogical heterogeneity of the subsurface environments considered for CO_2sequestration at different scales [e.g., *Landrot et al*., 2012] may magnify the impact of this two-way coupling between transport and reactive processes. *Ellis et al*. [2011] conducted a flow-through experiment to investigate evolution of a fractured carbonate (Amherstburg limestone) caprock during flow of CO_2-acidified brine. In this experiment, preferential dissolution of fast-dissolving calcite over slower-dissolving dolomite led to nonuniform dissolution of the fracture surface and an increase in roughness, exemplifying how dissolution patterns depend in a complex way on the mineral heterogeneity. Here a two-dimensional domain is constructed that is a conceptualization of the cross section in *Ellis et al*. [2011, Figure 6a] (Figure 10). The dimensions correspond to those of the cross section (0.165 × 0.165 cm), while the initial mineral assemblage is reconstructed from the final state assuming an initial fracture aperture of 173.9 μm and the presence of bands of pure calcite and pure dolomite initially. The domain is discretized with 64 × 64 cells for a resolution of 25.78 μm. A constant flow rate is prescribed at the inlet boundary such the initial velocity at the inlet is that reported in the experiments (110 cm/h). Due to widening of fracture aperture at the outlet, fluid velocities evolve in the domain during the simulation. The inlet boundary condition is obtained from the brine used in the experiment. This brine is representative of deep saline brines saturated with CO_2, resulting in a pH of 4.3, at 27°C and 10 MPa (Table 3). The rate constants used for calcite dissolution are 0.083, 1.1×10^{-4}, 1.5×10^{-5} mol m^{-2} s^{-1} for k_1, k_2, and k_3, respectively (equation 8) [*Deng et al*., 2015], which were derived from data of *Pokrovsky et al*. [2005]. The use of *Pokrovsky et al*. [2005] data at the pore scale has been shown to produce rates within a factor of 1.8 in the high pCO_2 experimental/modeling study of *Molins et al*. [2014]. In addition to calcite dissolution, dolomite dissolution is also considered with the rate expression and stoichiometric relationship as follows [*Pokrovsky et al*., 2005; *Deng et al*., 2016]:

$$r_m = k_4 a_{H^+}^{0.5}\left(1-\frac{a_{Ca^{2+}}a_{Mg^{2+}}a_{CO_3^{2-}}^2}{K_{s,dol}}\right), \quad (12)$$

$$CaMg(CO_3)_2(s) \rightarrow Ca^{2+} + Mg^{2+} + 2CO_3^{2-} \quad (13)$$

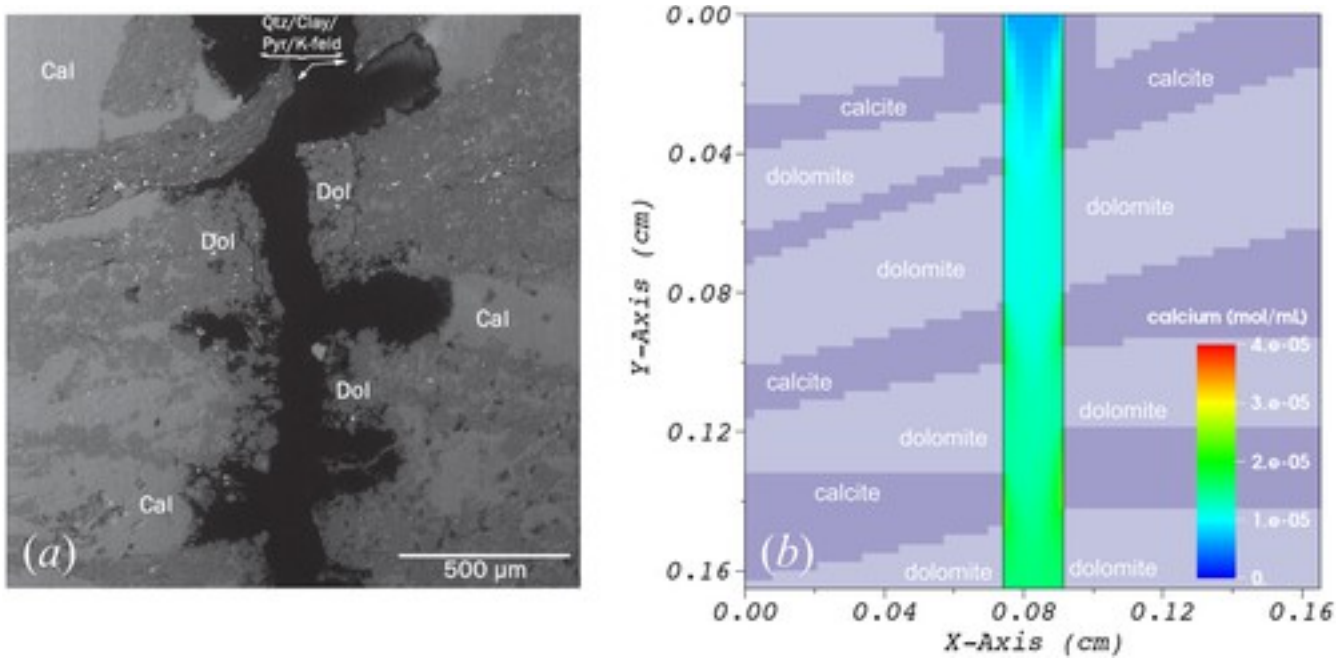

Figure 10
Open in figure viewerPowerPoint

(a) BSE image showing preferential dissolution of calcite on a fracture surface at the end of the experiment of Ellis and coworkers [from *Ellis et al.*, 2011]. (b) Simulation domain in the current work showing the initial mineral composition and geometry, and the calcium concentrations in the fracture at steady state conditions for reactive transport.

Caption

Table 3. Solution Parameters Used for the Initial and Inlet Boundary Conditions in the Fracture Simulation

Parameter	Value
pH	4.3
CO_2	0.98 mol/kgw
Ca	6.4×10^{-3} mol/kgw
Mg	1.8×10^{-2} mol/kgw

Parameter	Value
Na	1.0 mol/kgw
SO_4^{2-}	1.1×10^{-2} mol/kgw
Cl	1.0 mol/kgw

In the simulation, the conditions are very far from equilibrium both for dolomite and for calcite such that the near-equilibrium terms do not play a role. The rate constant k_4 is equal to 4.5×10^{-4} $mol/m^2/s$ [*Pokrovsky et al.*, 2005].

The difference between calcite and dolomite intrinsic rates causes the evolution of the fracture geometry to be dependent on the initial composition of the matrix. Where calcite is exposed to the flowing fluid, the fracture surface recedes rapidly while dolomite surfaces barely recede over the same time scale.

These results are qualitatively similar to what was observed by *Ellis et al.* [2011]. However, in comparison to observations by *Ellis et al.* [2011], the simulated mineral surface evolution rates are significantly faster. A quantitative comparison with effluent concentrations to calibrate the model was not performed as these data were not available from the experiment in *Ellis et al.* [2011]. This discrepancy is attributed to the simplifying assumptions in this simulation that focuses on a small 2-D section of a much larger 3-D fracture, and to a lesser extent to uncertainty in rate parameters. In the experiment, fluids in contact with this particular section (2 cm away from the inlet) were likely much closer to equilibrium than assumed in the simulation because of the consumption of reactants and transport of products in the first 2 cm of the domain.

The simulated average calcite dissolution rate decreases with time as indicated by decreasing effluent calcium concentrations (Figure 11). As calcite dissolution proceeds, calcite reactive surfaces are further away from the fracture channel, leading to an increase in the diffusive

limitation to the rate of calcite dissolution. Where the calcite bands have dissolved, fluid velocities are significantly lower than in the fracture (Figure 11) and transport is dominated by diffusion. The diffusive Damköhler number for calcite (Da_N, with L = aperture based on calcite surface) increases by a factor of 3 from 0.43 initially (Table 2) to 1.27 after 24 h, an additional indication that calcite rates become increasingly limited by diffusion. The thinner the calcite bands were initially, the slower the fluid velocity is within these dissolved regions. Because of this, the rate the calcite bands recede is slightly slower in the thinner bands than in the wider ones. Overall, this increasing diffusive limitation causes the effective rate to decrease. At the same time, calcite depletion uncovers more of the dolomite when the old calcite-dolomite interfaces are exposed to the fluid, increasing the surface area of dolomite available for reaction. This process is captured naturally by the model because the surface area is calculated as the interfacial area between the fluid and the solid. Thus, effluent magnesium concentrations increase with time (Figure 11). The reactive transport regime associated with dolomite, however, does not evolve as the fracture aperture where lined by dolomite does not change significantly.

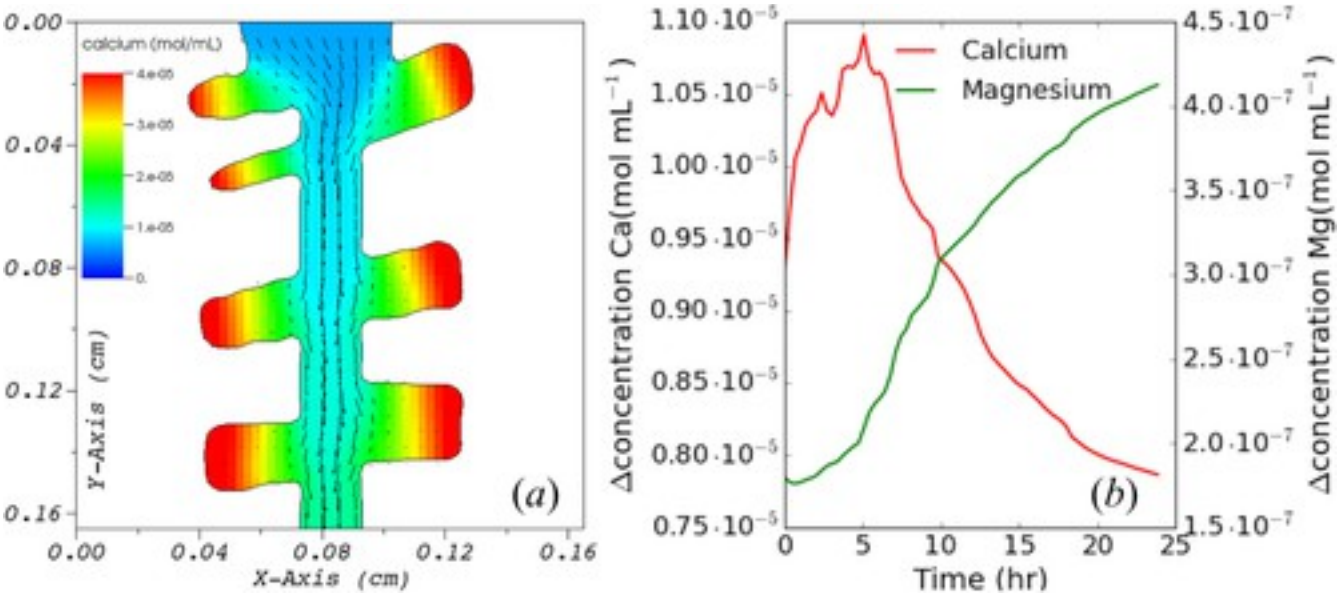

Figure 11
Open in figure viewerPowerPoint
(a) Simulated fracture geometry at 24 h showing calcium concentrations within the fracture aperture and local flow velocities in arrows. (b) Changes in effluent calcium and magnesium concentrations over time.

Caption

5 Discussion and Conclusions

The simulations presented here demonstrate that the evolution of the texture of the pore-scale domains depends on the reactive transport regime, the initial pore structure, and the mineral composition of the solid phase in each case. The simulations focused on the dissolution of calcite and dolomite owing to their role in carbon sequestration scenarios. Carbonate minerals are examples of primary minerals that can be a source of cations and alkalinity that drive the secondary mineral precipitation required for mineral trapping. Carbonate formations are investigated in their role as caprocks, e.g., Amherstburg limestone formation [*Ellis et al*., 2011], but also as reservoirs, often associated with oil fields, e.g., the Duperow formation [*Deng et al*., 2016]. These formations typically display mineral heterogeneity that control their evolution at the pore scale [*Ellis et al*., 2011; *Deng et al*., 2016].

The evolution of individual single-mineral crystals is a function of both the local flow and the reactive transport regime. Calcite dissolution is a relatively fast reaction and for the crystal size considered (100 μm in radius, $Da_{II}=7.6$), diffusive boundary layers developed around dissolving grains and diffusion limitation to rates was observed. On the grain surfaces exposed directly to the influent solution, reactions are relatively fast, while they are slower on downgradient surfaces. Thus, as the grain dissolves, its center of mass of the grain moves downgradient and this tendency increases at faster flow rates. This is in agreement with the results of *Rycroft and Bazant* [2016], who used an analytical solution to solve for advection-diffusion-limited dissolution of a cylindrical object being eroded by two-dimensional potential flow. However, the main difference is that in *Rycroft and Bazant* [2016] the cylindrical grain preserves its shape as it evolves. At relatively fast flow rates (small Da_I numbers), the grain evolves to an oblong shape. Under these conditions, diffusion limitation is only partial on the grain surfaces exposed directly to the influent solution, while on downgradient surfaces the reaction is slower and diffusion limits the reaction rate to a larger extent. In this case, concentrations at the surface tend to equilibrium. In *Rycroft and Bazant* [2016] the solution is obtained assuming diffusion-limited conditions, i.e., each fluid particle annihilates a solid particle upon contact with the grain. Therefore, it is only comparable to the two simulations with slow flow rates, which also show that the grain shape retains a cylindrical shape as it evolves and concentrations at the surface remain close to equilibrium values. Under mixed diffusion-surface control the grain shape evolution reflects the local flow conditions around the crystal. Faster dissolution is observed where flow velocities are fast and boundary layers are thin such as in pore throats or upgradient faces.

The local evolution of each crystal, however, is also tied to the grain-pack scale as the reactive transport regime evolves. As noted by *Pereira Nunes et al*. [2016], the evolution of a porous

medium does not depend only on the reactive transport regime (e.g., as expressed by the Péclet and Damköhler numbers) but also on the initial pore structure of the medium. In the simulation presented here, only one of the three domains considered showed an unstable evolution (this domain initially had a relatively fast flow path). This took place only under the slower flow rate, i.e., under relatively more transport-limited conditions, but not at the faster flow rate where the Damköhler number was lower. This development of a preferential flow path results in an increase in fluid velocity locally. In this region, the fluid velocities may be such that individual crystals evolve to have elongated shapes. In the microfluidic experiments of *Song et al*. [2014], fabricated by etching microchannels in a calcite rock sample, it was observed that the evolution of each individual grain depended on the local flow velocity, but also on whether reactive surfaces showed crystallographic etching (following calcite cleavage planes) or isotropic-like etching (against the cleavage plane). Given our model only considered uniform reactivity on all grain surfaces, results here suggest that the contribution of the local flow velocity alone to nonuniform or preferential dissolution of single crystals could be significant when fluid velocity increases locally where preferential flow paths developed.

Preferential dissolution may also occur due to mineralogical heterogeneity when some minerals are more reactive than others. Locally, this also affects the evolution of the texture of mineral surfaces. Observations by *Ellis et al*. [2011] of preferential dissolution of calcite leading to nonuniform aperture increases were qualitatively reproduced by our simulations, although fine-scale physical heterogeneity was not included in detail here. As the reactive surfaces of the fast-reacting calcite receded from the main flow path, diffusion limitations to surfaces increased, thus causing effluent concentrations of calcium to decrease as overall calcite dissolution slowed down. This is in agreement with the conceptual model proposed by *Deng et al*. [2016] for a fractured core experiment similar to that of *Ellis et al*. [2011]. In *Deng et al*. [2016], the diffusive limitation to the rate was modeled using a Darcy-scale continuum representation of a reacted layer, depleted of calcite, through which reactants and products had to diffuse. The diffusive limitation included both the effect of the distance between the main flow channel and the calcite surfaces, but also the tortuosity of the diffusive pathways. Here due to the initially banded structure in our pore-scale model, the effect is mostly due to the increase in the diffusive distance. However, the decrease in effluent calcium and associated increase in effluent magnesium is consistent with results from *Deng et al*. [2016]. These results highlight the difficulties of using dimensionless analysis to multimineral problems, as the evolution of the medium texture depends on the full range of Damköhler numbers characterizing the heterogeneous medium. This implies not only one for each mineral, but possibly more than one

because as the pore space evolves, dissolution may become limited by diffusion rather than by advective processes.

Reaction rate parameters for the dissolution of calcite and dolomite were sourced from literature values used in earlier pore-scale studies. These studies showed successful model validation against experimental results. Uncertainty in the rate values is thus expected to be within an order of magnitude or less in the results presented here. Significantly different rates—or if other minerals with different reactivity were considered—would have the effect of shifting the dimensionless Damköhler number analysis discussed above. For the same flow rate, slower-reacting minerals (e.g., silicates) would be less subject to transport limitations to rates at the grain scale, and less likely to develop preferential dissolution pathways at the grain-pack scale considered in this study.

Flow velocities considered here are relatively fast compared to natural conditions (typically slower than 0.001 cm/s). Results are thus applicable in regions of the plume where flow is significantly affected by the injection of CO_2, but also near leakage pathways where flow is relatively fast. In these areas, unstable dissolution at the gran-pack scale may only be observed when the initial structure contains fast flow paths. The local evolution of individual grains and pore throats, however, is expected to be nonuniform as some surfaces are subject to surface-controlled dissolution and others to diffusion-controlled dissolution. In regions that experience slower-fluid velocities the evolution depends on the solution degree of saturation with respect to the native minerals. Far-from-equilibrium conditions are expected to result in unstable evolution where dissolution is focused in faster-flowing pathways. Dissolution instabilities may in turn result in the nonuniform of evolution of individual grains in these regions.

The simulations presented here demonstrate the ability of the pore-scale model to capture the evolution of relatively geometrically simple—albeit very finely resolved—computational domains. In particular, the current model is a novel application of the general embedded boundary method for time-dependent domains presented in *Miller and Trebotich* [2012]. Assuming that geometry evolution is significantly slower than the other processes makes it possible to simulate these processes over relatively long time scales characteristic of geological media. Since calcite dissolution is a relatively rapid reaction and flow conditions considered here include some that are fast compared to natural flow conditions, the resulting mineral-fluid interface rates obtained in this manuscript are already among the fastest in subsurface applications. Therefore, the operator-splitting approach is expected to be applicable in most scenarios in subsurface problems where slower rates are common. Further, as noted above, effective reaction rates at mineral surfaces are the result of the interplay between transport and

reactive processes. Thus, for minerals with greater intrinsic rates, surface rates are likely to be limited by transport control rather than by reaction kinetics. This would result in slower effective rates, implying that even faster flow rates, possibly in the turbulent regime, would be necessary to observe fast mineral-fluid interface rates. In this scenario, however, the time-stepping approach would need to be adjusted such that flow, reactive transport, and boundary displacement were solved over the same time step, i.e., $\Delta t = \min \{\Delta t_V, \Delta t_A, \Delta t_B\}$.

The high-performance tools used in the numerical implementation of this model [see, e.g., *Trebotich et al*., 2014] make it possible to extend this work to simulate the processes in the physically and mineralogically complex media that make up natural subsurface materials. These tools will allow for simulation of large experimental data sets such as those in *Ellis et al*. [2011] or *Deng et al*. [2016], which require high-resolution and large-computational meshes of over 50M grid points, and ultimately allow for the evaluation of model results by comparison with measured effluent data. Increasingly, experimental results also make it possible to improve model representation of pore-scale reactive transport. For example, while physical and mineralogical heterogeneity was considered here, results from *Song et al*. [2014] suggest that inclusion of nonuniform or heterogeneous reactivity on different surfaces of the same mineral may improve model predictions.

Acknowledgments

This material is based upon work supported as part of the Center for Nanoscale Control of Geologic CO_2, an Energy Frontier Research Center funded by the U.S. Department of Energy, Office of Science, Office of Basic Energy Sciences under award DE-AC02-05CH11231. This research used resources of the National Energy Research Scientific Computing Center, a DOE Office of Science User Facility supported by the Office of Science of the U.S. Department of Energy under contract DE-AC02-05CH11231. The data used are listed in the figures, references, and tables.